American Journal of
Biomedical Science & Research

www.biomedgrid.com
ISSN: 2642-1747

Research Article

Discovery of QL-448B As a Novel Small Molecule Inhibitor that Suppresses Ovarian Cancer Growth and Metastasis by Retarding mRNA Decay of Oxidative Phosphorylation

Cancan Zhang[1†], Jinghai Gao[4†], Zhiyong Wu[8†], Xiaoge Ni[4], Chunlin Tao[4], Liwen Qin[5], Zhigang Zhang[7], Yihua Chen[5,6*], Rong Zhang[3*] and Tingyan Shi[2*]

[1]*Department of Obstetrics and Gynecology, Ruijin Hospital, Shanghai Jiao Tong University School of Medicine, Shanghai 200020, China*

[2]*Department of Gynecologic Oncology, Zhongshan Hospital, Fudan University, Shanghai 200032, China*

[3]*Shanghai Pudong New Area Health Care Hospital for Women & Children. 200120, China*

[4]*The Third School of Clinical Medicine, Southern Medical Universit,Shanghai, China*

[5]*Shanghai Key Laboratory of Regulatory Biology, Institute of Biomedical Sciences and School of Life Sciences, East China Normal University, Shanghai 200062, China*

[6]*School of Pharmaceutical Science and Yunnan Key Laboratory of Pharmacology for Natural Products and College of Modern Biomedical Industry, Kunming Medical University, Kunming, Yunnan 650500, China.*

[7]*State Key Laboratory of Oncogenes and Related Genes, Shanghai Cancer Institute, Renji Hospital, Shanghai Jiao Tong University School of Medicine, Shanghai 200030, China*

[8]*Shanghai Obstetrics and Gynecology Hospital of Fudan University, Shanghai, China*

[†]*These authors contributed equally to this work.*

***Corresponding author:** Emmanuella I Ezebuiro, Department of Obstetrics and Gynaecology, University of Port Harcourt Teaching Hospital, Rivers State, Nigeria.

To Cite This Article: *Tingyan Shi, Department of Gynecologic Oncology, Zhongshan Hospital, Fudan University, Shanghai 200032, China, Rong Zhang, Shanghai Pudong New Area Health Care Hospital for Women & Children. 200120, China, Yihua Chen, School of Pharmaceutical Science and Yunnan Key Laboratory of Pharmacology for Natural Products and College of Modern Biomedical Industry, Kunming Medical University, Kunming, Yunnan 650500, China. Am J Biomed Sci & Res. 2025 28(2) AJBSR.MS.ID.003653,* **DOI:** 10.34297/AJBSR.2025.28.003653

Received: August 13, 2025; **Published:** August 20, 2025

Abstract

Ovarian cancer has the poorest prognosis among all gynecologic cancers, and there is an urgent need for new effective treatments. Poly(U) binding splicing factor 60 (PUF60), is a nucleic acid-binding protein which promotes mRNA decay of oxidative phosphorylation has shown promise as a target for ovarian cancer treatment. In this study, we screened more than three thousand compounds by structure-based virtual screening, identifying QL-448B as the top compound due to its potent inhibitory activity targeting PUF60. QL-448B significantly suppresses tumor growth and metastasis *in vivo* and extends survival of tumor-bearing mice, especially in cisplatin resistant ovarian cancer cells. Mechanistic studies revealed that QL-448B selectively inhibits PUF60's role in promoting mRNA decay of oxidative phosphorylation in ovarian cancer cells. This study introduces QL-448B as the first-in-class selective PUF60 inhibitor, offering a promising therapeutic candidate for ovarian cancer treatment.

Keywords: QL-448B, Ovarian cancer, PUF60, targeted therapy, mRNA decay, oxidative phosphorylation

Abbreviations: PUF60: Poly(U) binding splicing factor 60; PARP: poly (ADP-ribose) polymerase; BRCA1/BRCA2: Breast cancer 1/2; RBPs: RBPs: RNA-binding proteins; SF3B1: Splicing Factor 3B1; Py-tract: polypyrimidine-tract; HuR: Hu antigen R; OXPHOS: oxidative phosphorylation; SBVS: Structure-based virtual screening; FBS: fetal bovine serum; CCK-8: Cell Counting Kit-8; SPR: Surface plasmon resonance.

Introduction

Ovarian cancer is the most common malignancy among the three major gynecologic cancers, ranking third in incidence rate [1]. Surgery combined with platinum-based chemotherapy is a standard clinical treatment for ovarian cancer. Most patients initially respond well to first-line chemotherapy, however, over more than 60% patients experience recurrence, and many patients develop secondary resistance, leading to disease progression and seriously affecting the survival and quality of life [2]. Significant improvement in maintenance therapy has been achieved by incorporating inhibitors of poly (ADP-ribose) polymerase (PARP) molecules involved in the DNA damage-repair process, which have been approved for recurrent cases and recently in a first-line setting among women with BRCA1/BRCA2 mutations. Therefore, identifying new targets and overcoming chemotherapy resistance in ovarian cancer remains a major challenge in clinical treatment.

Protein–RNA interactions play a crucial role in various cellular activities, and their disruption can lead to numerous human diseases [3]. RNA-Binding Proteins (RBPs) interact with target mRNAs to regulate multiple cellular functions by increasing or decreasing mRNA stability [4]. The rapid progress in identifying small molecules that target RBPs and interact with RNA presents a novel strategy for discovering chemical probes [5-7]. The RNA-binding protein Hu antigen R (HuR) is a key post-transcriptional regulator involved primarily in messenger RNA (mRNA) turnover and translation. Several successful small molecules that have been experimentally validated to bind to the Hu antigen R (HuR) proteins *in vivo*, including embelin, okicenone, triptolide, leptomycin B, selinexor, KH-3 and derivatives, suramin, mitoxantrone, and DHTS. One ligand tested *in vivo*, MS-444, is currently undergoing preclinical studies. A phase I clinical trial of H3B-8800, an oral small molecule that binds Splicing Factor 3B1 (SF3B1), in patients with MDS, CMML, or AML showed an acceptable adverse event profile, predictable pharmacokinetics, and modulated splicing. Although this field is expanding, challenges remain in the discovery and characterization of small-molecule inhibitors of RBPs.

PUF60 was first identified as a polypyrimidine-tract (Py-tract) binding protein in 1999 [8,9]. It encodes an RNA-binding protein that has been identified as a component of the spliceosome and is involved in pre-RNA splicing regulation [9-11]. Interestingly, copy-number gain and/or elevated expression of PUF60 have been reported in multiple cancers [12-17]. Our previous research has shown that PUF60 is highly expressed in ovarian cancer, and that its high expression is associated with poor prognosis in patients. Mechanistically, PUF60 promotes mRNA decay of OXPHOS genes and the formation of P-bodies, ultimately reducing OXPHOS levels to support the rapid growth of OC cells [12], suggesting that PUF60 may be a novel therapeutic target for OC.

Structure-Based Virtual Screening (SBVS), also known as molecular docking, has been increasingly applied to discover small-molecule ligands based on the protein structures in the early stage of drug discovery [18, 19]. The most significant advantage of molecular docking is its ability to effectively and efficiently identify novel chemotypes from a large chemical library against a target of interest. Furthermore, SBVS will boost hit identification in the immediate future, thanks to the advancements in several areas, including protein structure prediction, allosteric binding site identification, docking library augmentation, sampling and scoring algorithms, and post-processing strategies.

In the current study, we screened 3470 compounds of Targetmol Bioactive Compound Library and subsequently assessed their effects with a growth assay. To generate more potent bioactive candidates, we optimized the analogs of the initially screened inhibitors and discovered a new small molecule inhibitor-QL-448B. *In vivo* experiments, QL-448B could inhibit tumor growth of subcutaneous transplant tumors and the lung metastasis of OC cells. Subsequently, QL-448B retards mRNA decay of OXPHOS genes caused by the increase of PUF60. In addition, we found that compared to platinum or paclitaxel sensitive cells, PUF60 is highly expressed in drug-resistant cells, and QL-448B tends to have stronger inhibitory ability on drug-resistant cells. All the above experimental results indicate that QL-448B may be a novel targeted small molecule inhibitor for clinical OC treatment.

Materials and Methods

Cell Lines and Cell Culture

Human ovarian cancer cell lines OVCAR8, OVCAR3, OVCAR5, ES-2, SKOV3-IP, SKOV3-TR, COCL-Cisplatin-sensitive, COCL-Cisplatin-resistant, normal human ovary cell line IOSE-80, Human Embryonic Kidney 293T (HEK293T) cells were all preserved in Shanghai Cancer Institute, Ren Ji Hospital, School of Medicine, Shanghai Jiao Tong University. OVCAR8, OVCAR3, OVCAR5, SKOV3-IP · SKOV3-TR, COCL-Cisplatin-sensitive, COCL-Cisplatin-resistant were cultured in RPMI 1640 containing 10% Fetal Bovine Serum (FBS), 2 mM glutamine and 1% Penicillin/Streptomycin (P/S). ES-2 and HEK293T were cultured in Dulbecco's modified Eagle's medium containing 10% Fetal Bovine Serum (FBS) and 1% P/S. All cells were incubated at 37°C in a humidified atmosphere containing 5% CO2.

PUF60 Knockdown

The sequences of the short hairpin (sh)RNAs targeting PUF60 were sh-1, 5′-GCTACGGCTTCATTGAGTACG-3′ and sh-2, 5′-CTGAGACTCATAAGGCCATCC-3′. The shRNA plasmids and control plasmid were purchased from GenePharma (Shanghai, China). All these plasmids were packaged into virus particles using HEK 293T cells and the viral titers were determined. Then the target cells were infected with 1×108 lentivirus-transducing units with 6μg/mL polybrene (Sigma-Aldrich, St. Louis, MO, USA). The infected cells were then screened with 2μg/mL puromycin

after 72h. The efficiency of the knockdown or overexpression was verified by western blotting.

Viability Assays

All ovarian cancer cells or normal human ovary cells were cultured in 96-well plates at a density of 5000 cells/well. The cells were cultured for a certain time and incubated with various concentrations of small molecule inhibitors according to the requirements of the experiment. Each group contained five wells. 10 μl Cell Counting Kit-8 (CCK-8, WST-8, Dojindo, Japan) solution was added to each well after 24h or 48h. CCK8 was metabolized to produce a colorimetric dye that was read at 450nm using a microplate reader.

Western Blotting

Ovarian cancer cells were planted in 6-well plates at 1.4×10^5/ml. After being incubated with various concentrations of inhibitors for specified times, the protein was extracted via RIPA Buffer, including protease inhibitors and phosphatase inhibitors for 10 min at 4°C. Cell lysates were collected into EP tubes, centrifuged and the supernatant was collected, and protein lysates were quantified using Pierce™ BCA Protein Assay Kitt, then added loading buffer to the supernatant and boiled for 10 min at 100°C. The special protein was isolated via SDS-PAG gel, and detailed experimental methods were described in our previous study [20]. The specified primary antibodies are listed in (Table 1).

Surface Plasmon Resonance (SPR)

SPR was determined using a Biacore X-100 plus instrument (GE). PUF60 protein was immobilized on the sensor chip (CM5) using the amine-coupling method according to standard protocols. PUF60 protein was diluted in sodium acetate buffer, pH 4.5. ZK 756326 and GW9508 were diluted in PBS. To estimate the affinity, the binding assay was examined at 25°C using PBS buffer at a flow rate of 30μL min−. The affinity constants of binding were obtained using 1:1 Langmuir binding model via BIA evaluation software.

RNA Stability Assay and Sequencing for mRNA Life-time

OVCAR8 cells with siRNAs against PUF60 or NC were seeded into 6-well plates to get 50% confluency after 24h. Cells were treated with 10μg/ml actinomycin D and collected at indicated time points. The total RNA was extracted by the Simply P Total RNA Extraction kit (BSC52S1, BIOER) and analyzed by RT–PCR.

The turnover rate and half-life of mRNA were estimated according to a previously published paper [21]. As actinomycin D treatment results in transcription stalling, the change in mRNA concentration at a given time (dC/dt) is proportional to the constant of mRNA decay (*K*decay) and the mRNA concentration (*C*), leading to the following equation:

$$dC/dt = -K\text{decay}C$$

Thus, the mRNA degradation rate *K*decay was estimated by:

$$\ln(C / C0) = -K\text{decay}t$$

To calculate the mRNA half-life (t), when 50% of the mRNA is decayed (that is, $C/C_0 = 1/2$), the equation was:

$$\ln(1/2) = -K\text{decay}t1/2$$

From where:

$$t1/2 = \ln2/K\text{decay}$$

Colony Formation

Tumor cells were seeded into 6-well plates, allowing attachment overnight. Different concentrations of QL-448B were added for 1-week incubation. Then colonies were fixed by 4% paraformaldehyde and stained with 0.2% crystal violet. Images were photographed using a digital camera, and colonies were quantified by manual counting.

Ovarian Cancer Tumor Xenograft Model

BALB/c-nude, female, 6- to 8-week-old mice were obtained from SLAC, Shanghai, China. All animal experimental protocols were approved by the Animal Investigation Committee of the Institute of Biomedical Sciences. The xenograft tumor models were developed by injecting 5×106 cells in suspension into the right flank of a BALB/c-nude mouse while cells were suspended in PBS. Treatment began after the formation of tumor nodules. Tumor-bearing BALB/c-nude mice were randomly assigned to several groups and treated with intraperitoneal injection of compound or drug. The tumor volume and mouse body weight were measured once a week. The tumor volume was calculated using the following equation:

tumor volume (V) = length × width × width × 0.52

At the end of the experiment, the mice were euthanized by CO2. The tumors were removed and prepared for Western blot and IHC analyses.

Lung Metastasis Model of Human Ovarian Cancer

Four- to 6-week-old female nude mice were injected with 2×10^6 ovarian cancer (OVCAR8-luciferase) cells via the tail vein, On the next day, the mice were divided into three groups based on the mice's luminescence values. All mice in drug treatment groups were intraperitoneally injected with QL-448B (10 and 50 mg/kg/d), while the control group received an equivalent volume of vehicle. When the mice showed near-death indicators such as loss of mobility and body temperature drop, they were euthanized immediately in consideration of animal ethics. A single dose of 150mg/kg was intraperitoneally injected with D-luciferin, luciferin imaged using non-invasive bioluminescence imaging living imaging system (PerkinElmer, Waltham, MA) 10 minutes after the injection and analyzed using Living Image 3.0 software.

Pharmacokinetic Characteristics and Bioavailability in Mice

After single dose intravenous administration of compound QL-448B in female mice, blood samples were collected at different time points (5min, 15min, 30 min, 1h, 2h, 4h, 6h, 8h, 24h). LC-MS/MS was used to determine the concentration of the compound in mouse plasma and calculate relevant pharmacokinetic parameters.

Thermodynamic Solubility Determination

QL-488B sample powder was weighed into EP tubes and added 450μL pH2, pH 7.4, pH 9 buffer into the above EP tube to get a oversaturation suspension. Then, vortexed the solubility samples for at least 2minutes and shaked the EP tubes on a shaker for 24 hours at RT at the speed of 800rpm.Centrifuged 20min (eg.12000rpm) and filtrated the supernatant with 0.45μm filters for injection into HPLC system and calculated the concentration with standard curve.

Statistical Analysis

Experiments were carried out with three or more replicates. Statistical analyses were performed using Student's t-test. P values <0.05 were considered significant. The differences between control and experimental groups were determined by one-way ANOVA. Since treatment and time course were investigated, two-way ANOVA followed by post hoc tests was also applied. Data were expressed as as mean values with 95% confidence intervals and P<0.05 was considered significant. All analyses were performed using GraphPad Prism 10 software.

Results and Discussion

Results

Virtual Screening and Identification of Inhibitors Targeting PUF60

Our work has demonstrated that PUF60 exerts an oncogenic role in OC [12]. To further confirm the pivotal roles of PUF60 in ovarian cancer, a virtual screening was carried out to identify several small molecule compounds for future potential clinical treatment of OC through targeting PUF60. Unfortunately, the complete structure of the PUF60 protein has not yet been reported, and only 3 proteins containing a UHM domain (3UE2, 3US5 and 3DXB) have solved crystal structures and been reported in the Worldwide Protein Data Bank (PDB). Three parameters of the crystal structures, Resolution, R-value Free and R-value work, are commonly used to evaluate the quality of the crystal structure (Table 1). The smaller the values, the more reliable the crystal structure data; thus, 3UE2 was chosen as the preferred structure for PUF60 protein (Figure 1A). Then, we superimposed the three crystal structures, and the UHM structure of 3DXB was significantly different from the others (Figure 1B). Based on the above analysis, 3DXB was also chosen as an additional structure for virtual screening of the PUF60 protein.

Table 1: Virtual screening of chemical structures and related information of candidate compounds.

No.	ID	CHEMPLP	LE_CHEMPLP	Chemscore	LE_Chemscore	M.w.	logP(o/w)	logS	SlogP	Target
1	T2539	82.4825	3.7492	34.7066	1.5776	307.478	3.916	-4.9884	3.2042	3DXB
2	T1930	57.5637	3.198	30.2602	1.6811	240.35	3.532	-3.4073	3.6219	3DXB
3	T1471	64.9803	3.0943	29.4448	1.4021	333.883	5.666	-5.6032	1.7304	3UE2
4	T0348	69.4712	2.8946	30.7781	1.2824	364.873	3.658	-4.3991	3.0329	3DXB
5	T0173	63.2194	2.8736	28.7346	1.3061	335.875	5.142	-4.4742	4.3225	3DXB
6	T0450	62.2339	2.8288	26.2327	1.1924	309.331	4.757	-4.2284	4.842	3UE2
7	T1308	54.5582	2.7279	28.9752	1.4488	305.849	5.172	-4.8686	4.5601	3UE2
8	T1781	70.8567	2.7253	28.2463	1.0864	347.414	4.841	-4.6447	5.3746	3DXB
9	T3360	69.6507	2.6789	29.5316	1.1358	429.388	4.539	-5.4814	4.4758	3DXB
10	T0324	58.7375	2.6699	27.2566	1.2389	337.847	4.396	-4.2878	3.7687	3DXB
11	T2254	53.1714	2.6586	27.9985	1.3999	300.406	3.158	-5.3514	3.8548	3DXB
12	T2342	61.0784	2.6556	26.8787	1.1686	314.36	3.127	-4.0696	3.045	3DXB
13	T0157	66.3426	2.6537	25.747	1.0299	384.904	3.48	-4.0785	3.1891	3UE2
14	T0726	61.0349	2.6537	29.5838	1.2863	345.874	4.877	-5.0186	4.4835	3UE2
15	T0214L	65.7697	2.6308	29.9327	1.1973	392.907	4.388	-5.8545	3.9615	3DXB
16	T0919	64.6912	2.5876	21.6427	0.8657	387.829	5.86	-5.9745	5.1965	3DXB
17	T2343	69.8455	2.5869	26.3955	0.9776	372.456	1.835	-3.9819	3.7914	3DXB
18	T0866	64.1994	2.568	24.6108	0.9844	341.451	3.542	-3.5448	3.2414	3UE2
19	T2385	69.4156	2.4791	30.384	1.0851	404.458	2.71	-4.591	2.2416	3DXB
20	T1275	51.6892	2.4614	27.9724	1.332	377.465	2.018	-3.536	1.7787	3UE2
21	T2549	53.6695	2.4395	31.1095	1.4141	370.671	9.097	-6.5157	4.0677	3DXB

22	T3185	56.1072	2.4394	27.0693	1.1769	312.304	2.674	-4.0125	3.5141	3DXB
23	T1781	63.1639	2.4294	29.4316	1.132	347.414	4.841	-4.6447	5.3746	3UE2
24	T1991	66.3708	2.3704	32.0466	1.1445	411.864	5.837	-7.2056	6.1739	3DXB
25	T3360	59.785	2.2994	30.3326	1.1666	429.388	4.539	-5.4814	4.4758	3UE2
26	T2301	56.0019	2.2401	28.7318	1.1493	331.35	4.127	-4.6116	3.146	3UE2
27	T2306	66.6607	2.1503	28.854	0.9308	433.576	4.549	-5.938	4.8478	3DXB
28	T6620	57.8906	2.1441	28.4094	1.0522	378.899	6.168	-6.2277	5.463	3UE2
29	T1677L	82.316	2.0077	36.6849	0.8948	608.178	9.268	-9.1714	8.0203	3UE2
30	T2555	65.0881	1.9724	28.5185	0.8642	564.565	5.481	-6.6119	1.9823	3DXB
31	T0068	58.8796	1.9627	32.051	1.0684	510.452	5.986	-7.1961	6.2236	3UE2
32	T0835	54.7467	1.9552	29.0871	1.0388	371.524	6.698	-6.8304	5.8134	3UE2
33	T2280	52.4156	1.872	28.2819	1.0101	373.496	6.122	-6.3375	5.1768	3UE2
34	T2562	57.8102	1.7518	30.1706	0.9143	442.475	6.23	-6.2814	3.2524	3UE2

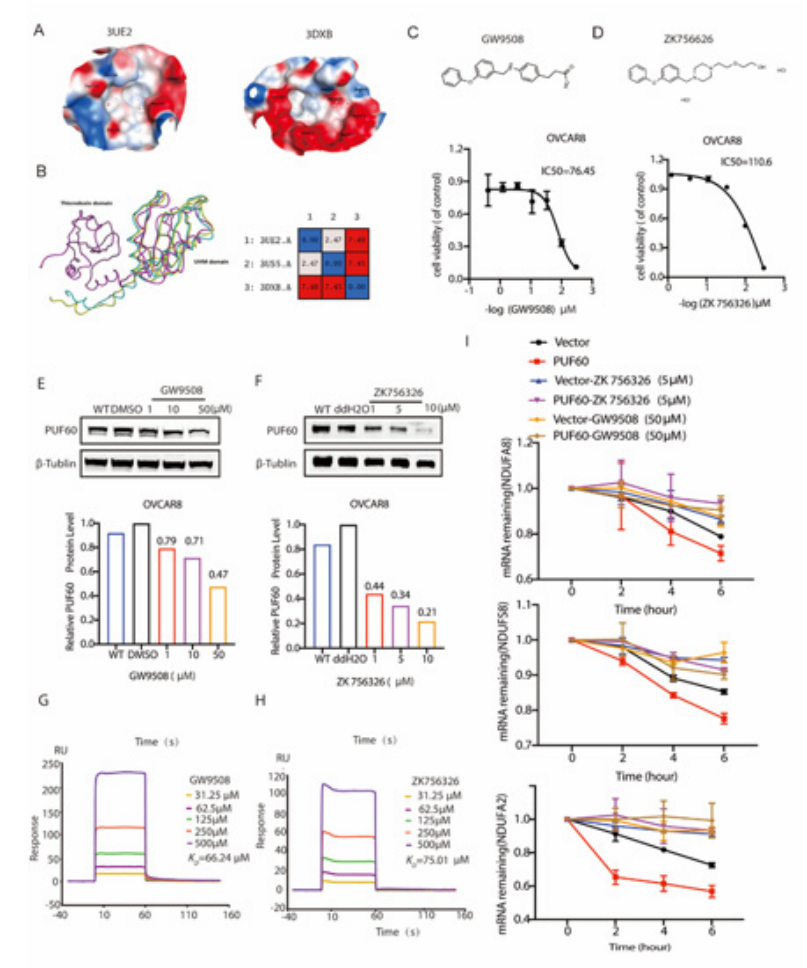

Note*: (A), (Left) Three crystal structures overlay. Cyan blue, PDB code: 3UE2; Yellow, PDB code: 3US5; Purple, PDB code: 3DXB. (Right) Comparison of RMSD values of three crystal structures overlap. Three PUF60 protein crystal structures information. (B), Prediction of UHM domain binding pocket electrostatic surface map in 3UE2 and 3DXB. White, hydrophobic neutral; Red, negative; Blue, positive). (C), Schematic diagram of small molecule virtual screening process targeting PUF60 protein. (D), Chemical structures of ZK 756326 and GW 9508 and their IC50 in OVCAR8 cells. (E), Detection of PUF60 protein expression after treatment of ovarian cancer cells with different concentrations of ZK 756326 and GW 9508. Left: western blot gels. Right: Protein quantification. treatment group values were compared with the control group. (F), Detection of affinity between PUF60 protein and ZK 756326/GW 9508 through SPR. (G), mRNA stability measurement in control and PUF60 overexpressed OVCAR8 cells after ZK 756326 and GW 9508 treatment.

Figure 1: Virtual Screening and identification of inhibitors targeting PUF60.

Then, we performed structure-based virtual screening using molecular docking, including prefiltering based on molecular properties, evaluation of molecular docking and scoring functions, protein binding pocket property matching analysis, combined with pattern analysis, etc. Ultimately, 32 candidate compounds were selected from the Targetmol Bioactive Compound Library containing 3470 compounds (Table 1). Among these compounds, only two were present in two structural parallel screenings: ZK 756326 and GW9508. Then, based on their IC50 values (Figure 1C-D), we treated OC cells with different concentrations of ZK 756326 and GW 9508, and we found that both compounds could significantly decrease the protein expression of PUF60 (Figure 1E-F). The binding between PUF60 and ZK 756326/GW 9508 was examined by surface plasmon resonance (SPR) assay. Binding of PUF60 with ZK 756326 and GW 9508 showed time-dependent saturation and the KD value were about 75.0μM and 66.21μM (Figure 1G-H).

Our previous research had demonstrated that PUF60 promoted mRNA decay of mRNA transcripts involved in OXPHOS, so we investigated the effect of inhibitors on the function of PUF60 in promoting mRNA degradation. We added inhibitors to cells that overexpressed PUF60 and performed mRNA stability measurements. The results showed that overexpression of PUF60 accelerated the mRNA decay of target genes, and the addition of ZK 756326 and GW 9508 alleviated the degradation rate of the target genes (Figure 1I). In summary, our results demonstrated that ZK 756326 and GW 9508 are small molecule inhibitors that provide a preliminary foundation for further intensive study.

Identification Of QL-448B As a Novel and Potent PUF60 Inhibitor

Our research showed that the above ZK 756326 and GW 9508 significantly inhibit the expression of PUF60 and play a role in suppressing tumors. Their analogs in house compounds library of our research group were next selected to screen and modified, twenty derivatives were further synthesized and optimized based on the structure properties, and among them, five derivatives showed strong PUF60 protein inhibitory ability (Figure 2A). Those five derivatives were subsequently evaluated in a subscreen on cellular PUF60 inhibition and their effective inhibitory concentrations, three derivatives exhibited significant cellular PUF60 inhibition was thereby selected as a candidate for further evaluation (Figure 2B). We used the two OC cells to explore its inhibitory effect and found that QL-448B and QL-418, but QL-486, could dose-dependently inhibited PUF60 protein level (Figure 2C-E).

To determine whether three derivatives treatment could decrease the viability OC cells, we used two relatively highly expressed PUF60 cell lines, two low expression cells and one human normal ovarian epithelial cell line and found that QL-448B had a lower IC50 at a concentration of 18μM, whereas PUF60 low and normal ovary cells with IC50 values of more than 200μM; QL-418 showed similar results, but not in QL-486 (Figure 2F-I), which indicated that QL-448B effectively inhibited the growth of highly expressed PUF60 cells with fewer toxic side effects on normal cells.

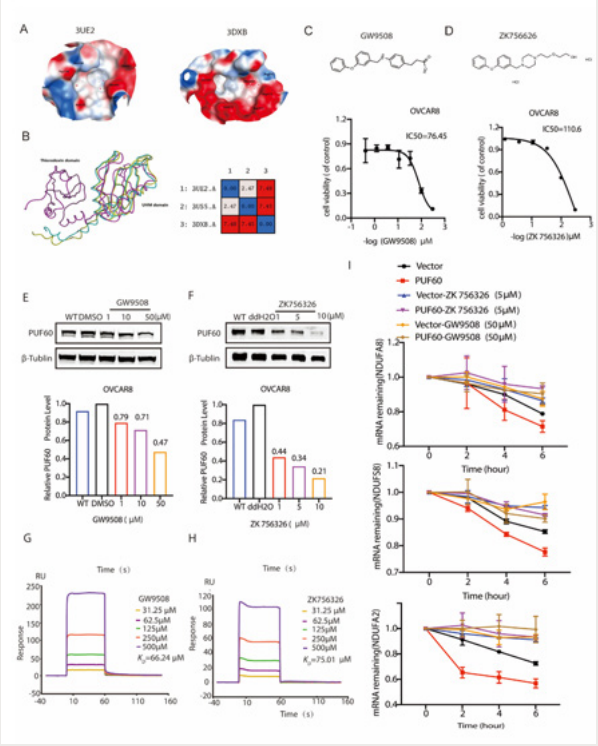

Note*: (A), Protein expression of PUF60 after treatment with 20 derivatives in OVCAR8, concentration is 5 μM. (B), IC_{50} five derivatives in OVCAR8 and ES-2 cells. (C-E), Upper: molecular structure of QL-448B, QL-418, QL-486. Lower: protein expression of PUF60 after different concentrations of QL-448B, QL-418, QL-486 to treat OVCAR8 and ES-2 cells. (F-I), PUF60 expression and IC 50 of QL-448B, QL-418, QL-486 in different cells.
Figure 2: Identification of QL-448B as a novel and potent PUF60 inhibitor.

QL-448B Inhibits mRNA Decay of Oxidative Phosphorylation in Ovarian Cancer Cells

To further investigate the specificity of inhibitors, we interfered PUF60 expression with Si-RNA in ovarian cancer cells and found that PUF60 knockdown in OC cells increased IC50 values of QL-448B, not QL-418, indicating that QL-448B is a specific inhibitor of PUF60 (Figure 3-A, Figure S1-A). The binding between PUF60 and QL-448B and QL-418 was examined by surface plasmon resonance (SPR) assay. Binding of PUF60 with QL-448B and QL-418 showed time-dependent saturation and the KD value were about 20.06μM and 42.8 μM (Figure 3B, Figure S1-B). Combining all the above results, we take QL-448B as the ultimate research target.

Our experiments have shown that PUF60 promotes the mRNA decay of oxidative phosphorylation genes. Therefore, we treated the over-expressing PUF60 and control cells with QL-448B to observe the effects of QL-448B on the mRNA stability. Over-expressing PUF60 promoted mRNA decay of oxidative phosphorylation genes such as NDUFA2, NDUFA8, and NDUFS8, QL-448B rescued accelerated mRNA degradation of target genes caused by overexpression of PUF60 (Figure 3C-D).

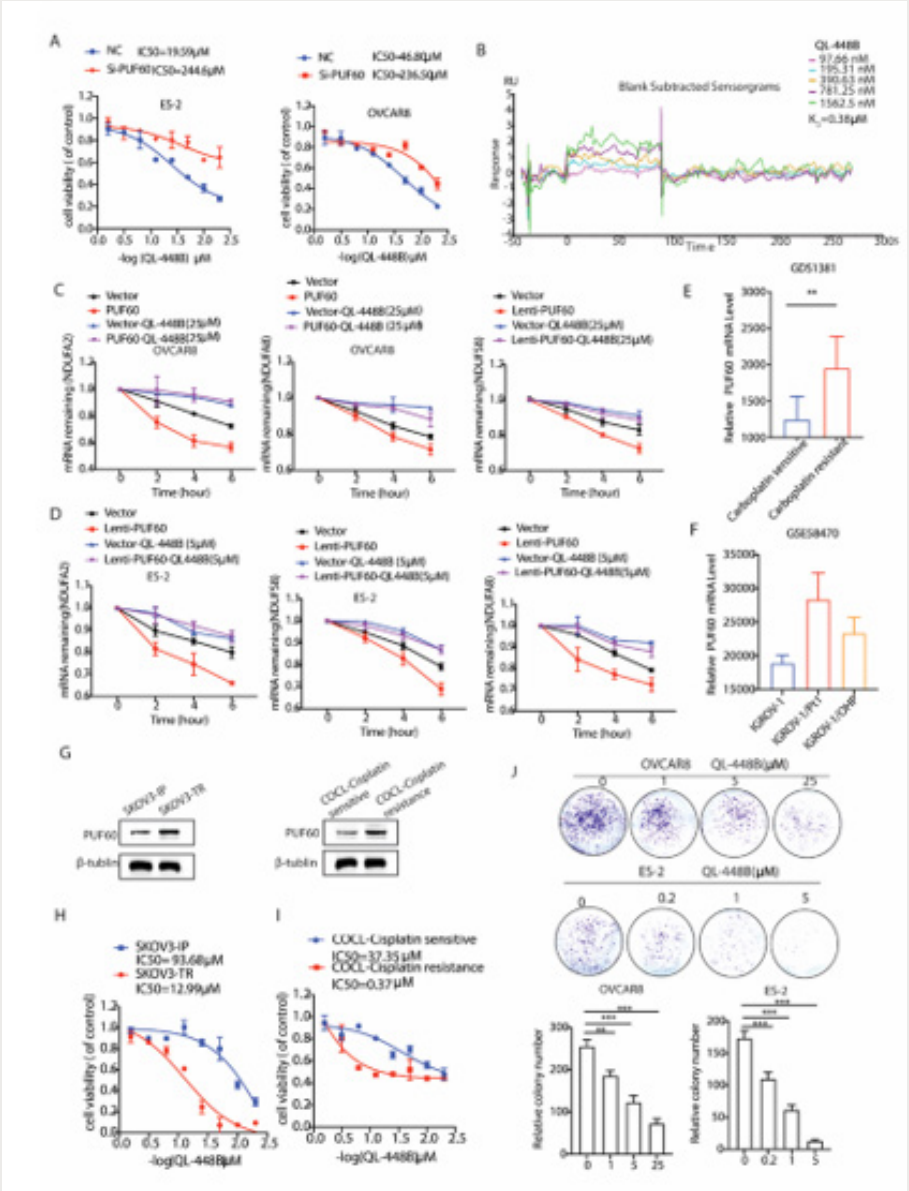

Note*: (A), IC50 of QL-448B in control and PUF60 knockdown OVCAR8 and ES-2 cells. (B), Detection of affinity between PUF60 protein and QL-448B through SPR. (C-D), mRNA stability measurement of NDUFA2, NDUFA8 and NDUFS8 in control and PUF60 overexpressed OVCAR8 and ES-2 cells after QL-448B treatment. (E-F), PUF60 expression in cisplatin-resistant samples from the GEO datasets. IGROV-/Pt1: Paclitaxel-resistant mutant cell line, IGROV-1/OHP: Paclitaxel-induced cell line. (G-I), PUF60 expression and IC50 of QL-448B in paclitaxel- and cisplatin-resistant cell lines. SKOV3-TR: Paclitaxel-resistant cell, SKOV3-IP: control. (J), Colony forming ability of OVCAR8 and ES-2 cells with QL-448B treatment or not at different concentrations.

Figure 3: QL-448B selectively inhibits the ability of PUF60 function on promoting mRNA decay of oxidative phosphorylation in ovarian cancer cells.

QL-448B Exhibited Stronger Inhibitory Ability in Chemotherapy Resistant Cells

Two factors of high OC morbidity and mortality are late detection and drug resistance. Although cisplatin-based chemotherapy improves overall and tumor-free survival, most patients who are treated eventually develop chemotherapy resistance, so solving the problem of chemotherapy resistance is the key to treating OC. Interestingly, our study showed that the expression of PUF60 was relatively high in cisplatin and paclitaxel-resistant samples and QL-448B showed stronger tumor suppressive ability in cisplatin and paclitaxel-resistant cell lines (Figure 3E-H).

QL-448B Suppressed Ovarian Cancer Cell Colony Formation

A colony formation assay was carried out in OVAR8 and ES-2 cells to evaluate the proliferative capacity and tumorigenicity of adherent tumor cells after QL-448B treatment. The results indicated that QL-448B dose-dependently inhibited the colony formation of OVAR8 and ES-2 cells (Figure 4J).

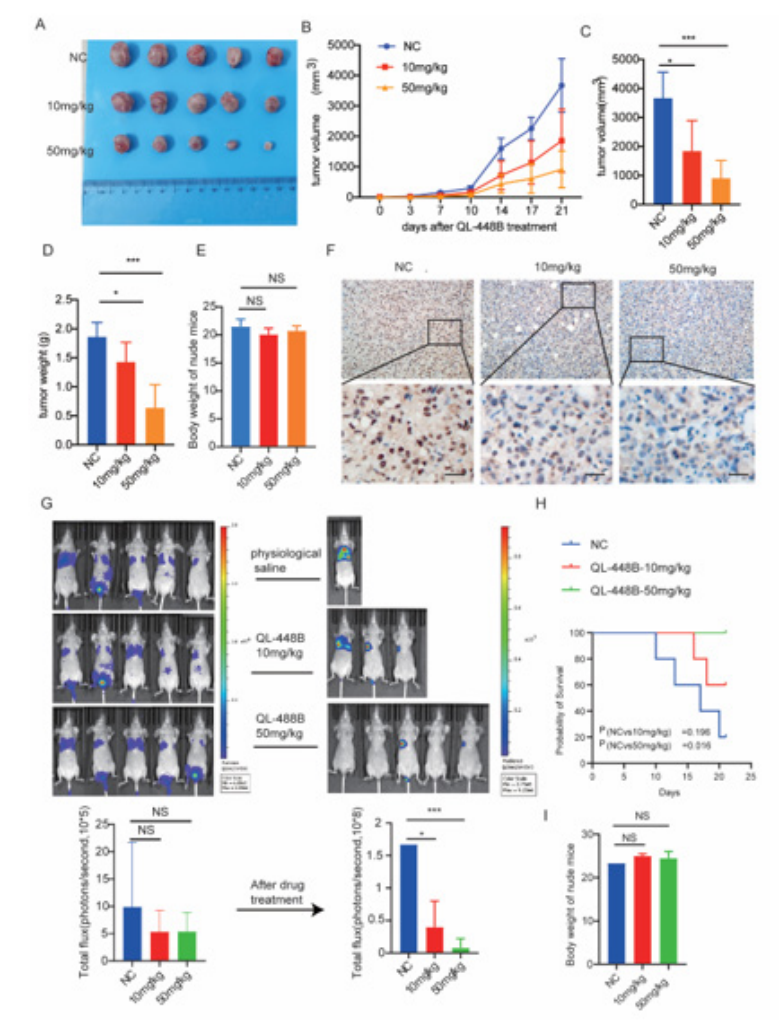

Note*: (A-B), Growth curve of subcutaneous xenografts in nude mice. (C-D), The tumor volume and weight of subcutaneously transplanted tumors in nude mice. (E), Body weight of nude mice. (F), PUF60 expression of in nude mice subcutaneously transplanted tumor. (G), The numbers of lung metastatic nodules were counted. The whole body IVIS images provided the quantification of bioluminescent signaling from the luciferase tagged tumor cells in each group. (H), The Kaplan–Meier survival curve. (I), Body weight of nude mice. Data shown are mean ± s.d. $p < 0.05$, *; $p < 0.01$, **; $p < 0.001$, ***; ns, not significant.

Figure 4: QL-448B prevents ovarian cancer growth and lung metastasis in vivo.

QL-448B Blocked OC Growth and Metastasis *In Vivo*

Subcutaneous xenograft mouse models were generated using OVCAR8 cell line, and the models were used to test the antitumor growth effects of QL-488B *in vivo*. We administered QL-488B to the mice by intraperitoneal injection. Mice were sacrificed and tumors were isolated after treatment with QL-448B (21 days) (Figure 4A). QL-448B treatment group significantly inhibited tumor growth compared with the control group according to the tumor

volume (Figure 4B-C). Consistently, the tumor weight significantly decreased in tumors compared to the control group after treatment with QL-448B (Figure 4D). Notably, compared to the 10 mg/kg group, 50mg/kg group showed a higher inhibitory effect on tumor growth (Figure 4A-D). Furthermore, no weight losses and drug-induced deaths of mice were observed in the QL-448B groups, implying the low toxic side effects of QL-448B (Figure 4E).

Our previous research has shown that PUF60 promoted lung metastasis of OC cells. So, lung metastasis mouse model by injecting OVCAR8-luc cells into nude mice via the tail vein. Fluorescence signals in the lungs were detected by IVIS. Once metastases were detected in the lung, 15 mice with metastases were randomized into three groups (n = 5 per group): (1) vehicle control group (DMSO); (2) QL-448B 10 mg/kg/day group and (4) QL-448B 50 mg/kg/day group (Fig. 4G). By day 20, the metastatic foci in control had grown to a relatively large size, but those in the QL-448B-treated groups, especially in 50 mg/kg/day group remained relatively small (Figure 4G). Kaplan-Meier curve analysis was performed. The survival times of mice in the QL-448B groups were longer than those of mice in the control groups (Figure 4H). 80% control mice were dead on the 20th day, which was generally caused by excessive lung colonization of the cancer cells. There is no significant difference in body weight among living animals (Figure 4I). Taken together, these findings indicated that QL-448B potently suppressed metastasis and significantly prolonged the survival of mice with metastatic OC *in vivo*.

Interestingly, the photon flux results indicated that 10mg/kg QL-448B entirely blocked signaling from all the distant metastatic sites (Figure 4G). Survival analysis showed that mice receiving 50 mg/kg QL-448B lived significantly longer than the 50mg/kg QL-448B and control group (Figure 4H). Furthermore, body weight measurements demonstrated no evident weight loss over the course of the treatment (Figure 4I). In summary, QL-448B treatment inhibited tumor growth and metastasis in a spontaneous mouse model.

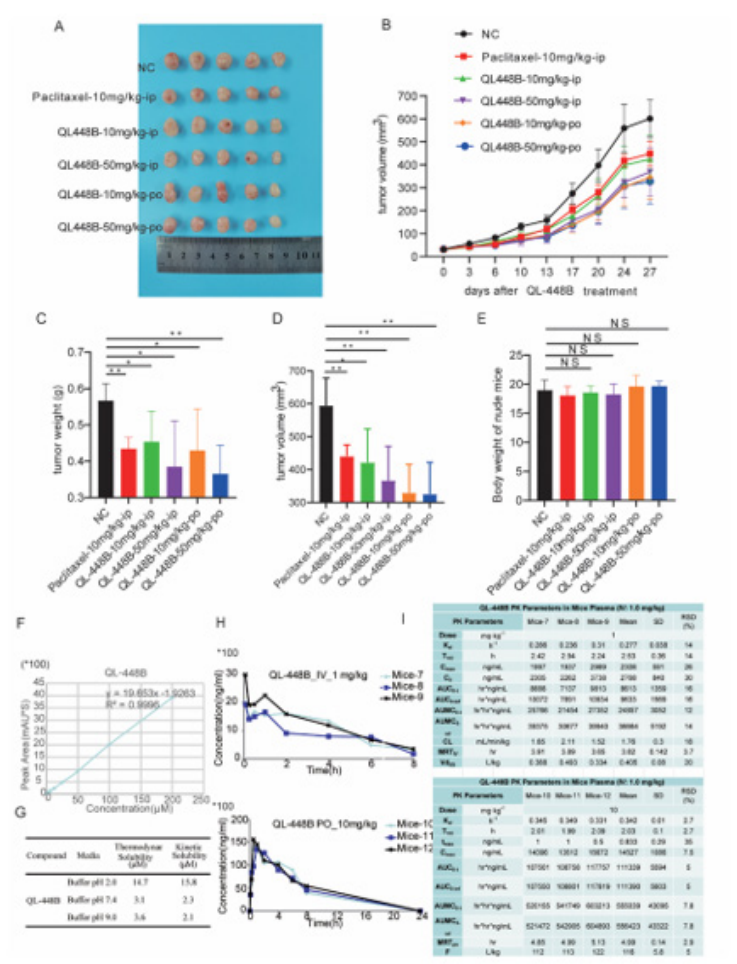

Note*: (A-B), Growth curves of subcutaneous transplanted tumors in each group. (C) Statistical analysis of tumor volume in each group. (D) Statistical analysis of tumor weight in each group. (E) Statistical analysis of nude mice body weight in each group. (F-G) The thermodynamic and kinetic solubility and of QL-448B. (H-I) Pharmacokinetic analysis of QL-448B by oral or intravenous injection. Data are presented as the mean ± SD. *p < 0.01; **p < 0.001; ***p < 0.0001.

Figure 5: The oral dosage form of QL-448B exhibited excellent pharmacokinetic effects.

The Oral Dosage Form of Ql-448b Exhibited Excellent Pharmacokinetic Effects

To further investigate the inhibitory effects of different formulations on OC, we conducted the following animal experiments. Subcutaneous xenograft mouse models were generated using SKOV3 paclitaxel sensitive cell lines, and the models were used to test the antitumor growth effects of QL-448B *in vivo*. Paclitaxel (10mg/kg/day), used for the first-line chemotherapy in OC, served as a positive control. The results showed that the tumor volumes of mice in the drug treated groups (compared with those of mice in the vehicle group) were significantly decreased by the administration of 10 or 50mg QL-448B per day. Further analysis revealed that comparing with the tumor volume of mice in Paclitaxel 10mg/kg ip group, mice in QL-448B 10mg/kg po group was significantly decreased, but there is no significant difference between oral administration and intraperitoneal injection (Figure 5C). The tumor weight significantly decreased in tumors compared to the control group after treatment with QL-448B or Paclitaxel, there is no significant difference between oral administration and intraperitoneal injection (Figure 5D). Furthermore, no weight losses and drug-induced deaths of mice were observed in the QL-448B groups, implying the low toxic side effects of QL-448B (Figure 5E).

To understand the absorption and distribution of drugs in the body, and optimize the formulation and administration of QL-448B accordingly. We tested the thermodynamic and kinetic solubility and of QL-448B has excellent thermodynamic and kinetic solubility (Figure 5E-G). Pharmacokinetic analysis showed that QL-448B exhibited excellent effects in mice (Figure 5H-I).

Discussion

PUF60 is prevalent highly expressed in a variety of human solid cancers. Our recent work suggested that PUF60 promotes the proliferation and migration of OC cells both *in vitro* and *in vivo*. Mechanistically, silencing of PUF60 enhanced the stability of mRNA transcripts involved in OXPHOS and decreased the formation of processing bodies (P-bodies), ultimately elevating the OXPHOS level. Thus, PUF60 is established as a promising therapeutic target for cancer treatment. In this study, a rational virtual screening strategy has been established and QL-448B, a novel PUF60 inhibitor was obtained from multiple manual screening.

PUF60 was initially discovered as a polypyrimidine-tract (Py-tract) binding protein in 1999 [8,9]. PUF60 contains two central RNA Recognition Motifs (RRMs) and a C-terminal U2AF-Homology Motif (UHM) [22]. PUF60-UHM binds to ULM sequences in the splicing factors SF1, U2AF65, and SF3b155. Compared with U2AF65-UHM, PUF60-UHM has distinct binding preferences to ULMs in the N terminus of SF3b155 [23]. PUF60 has homology to U2AF65, a general splicing factor that facilitates 3' splice-site recognition at the early stages of spliceosome assembly. PUF60 can functionally substitute for U2AF65 *in vitro*, but splicing is strongly stimulated by the presence of both proteins [10]. Owing to its important role in PUF60 function, the PUF60-UHM domain is turning into a feasible target for antagonizing PUF60. At present, there are no inhibitors targeting PUF60. Therefore, highly selective PUF60 inhibitors to treat ovarian cancer are urgently needed.

PUF60 protein is a novel target protein, and there are currently no publicly reported small molecule compounds targeting this protein, which is also the main difficulty of our virtual screening work. We conducted virtual screening using molecular docking based on two PUF60 protein structures (3UE2 and 3DXB) with UHM domains provided in the PDB database, including pre filtering based on molecular properties, evaluation of molecular docking and scoring functions, protein binding pocket property matching analysis, binding mode analysis, etc. Finally, 32 candidate compounds were selected from the Targetmol-Bioactive-Compound-Library containing 3470 compounds. It is worth noting that due to the differences in the binding pockets, the compounds virtually screened by 3DXB structure scored relatively higher. However, based on the parallel screening of two protein structures, there were only two compounds that appeared repeatedly, namely T1781-GW9508 and T3360-ZK 756326.

Further results indicate that GW9508 and ZK 756326 not only inhibit the proliferation of ovarian cancer cells, but also suppress the mRNA degradation of oxidative phosphorylation related genes caused by PUF60 overexpression.

Due to the weak inhibitory ability of GW9508 and ZK 756326 in ovarian cancer cells, we screened 20 analogs from our own small molecule inhibitor library based on their molecular structures. Among them, 3 compounds showed strong inhibitory ability, which attracted our attention. Notably, the binding affinities (KD), and growth inhibitory activity (IC50) of QL-448B were about 10 to 200-fold more potent than GW 9508 and ZK 756326 tested in this study.

Our previous reports have demonstrated that inhibiting PUF60 expression markedly suppressed ovarian cancer cell growth and lung metastasis. Mechanistically, silencing of PUF60 enhanced the stability of mRNA transcripts involved in OXPHOS and decreased the formation of processing bodies (P-bodies), ultimately elevating the OXPHOS level [12]. Indeed, our results demonstrated that QL-488B significantly blocked ovarian cancer growth, lung metastasis and prolonged tumor-bearing mouse survival. Further experiments clarified QL-488B suppress the mRNA degradation of oxidative phosphorylation related genes caused by PUF60 overexpression.

Platinum-based chemotherapy is the backbone of treatment for ovarian cancer, and although the majority of patients initially have a platinum-sensitive disease, through multiple recurrences, they will acquire resistance. Platinum-resistant recurrent ovarian cancer has a poor prognosis and few treatment options with limited efficacy. Despite the success of PARP inhibitors, treatment options are limited, particularly in the platinum-resistant setting. Novel biomarkers are needed to direct new treatments for ovarian cancer,

a disease for which the standard of care remains heavily focused on platinum-based chemotherapy. In this study, compared with wild-type cell lines, PUF60 is expressed higher in cisplatin resistant cells, and QL-448B exhibits higher inhibitory ability in resistant cells, indicating that QL-448B might be used for the treatment of chemotherapy resistance in ovarian cancer.

Conclusion

This study presents QL-448B as a highly potent and selective PUF60 inhibitor that markedly inhibited ovarian cancer growth and metastasis *in vitro* and *in vivo.* Furthermore, QL-448B exhibits higher inhibitory ability in cisplatin resistant cells. Our results laid a solid foundation supporting PUF60 as a promising drug target for ovarian cancer, and evaluated QL-448B as a potential candidate for ovarian cancer treatment.

Acknowledgements

This work was supported by the National Natural Science Foundation of China [Grant number 82173242 to T.Y. Shi ; Grant numbers 82472923 and 81974407 to R. Zhang] and Zhongshan Talent Program [Grant number 2021ZSGG14 to TS].

Conflict of Interest

None.

References

1. Siegel RL, Giaquinto AN, Jemal A (2024) Cancer statistics, 2024. CA Cancer J Clin 74(1): 12-49.
2. Alatise KL, Gardner S, Alexander Bryant A (2022) Mechanisms of Drug Resistance in Ovarian Cancer and Associated Gene Targets. Cancers (Basel) 14(24): 6246.
3. Zhao Y, Mir C, Garcia Mayea Y, Paciucci R, Kondoh H, et al. (2022) RNA-binding proteins: Underestimated contributors in tumorigenesis. Semin Cancer Biol 86(3): 431-444.
4. Li W, Deng X, Chen J (2022) RNA-binding proteins in regulating mRNA stability and translation: roles and mechanisms in cancer. Semin Cancer Biol 86(2): 664-677.
5. Wu P (2020) Inhibition of RNA-binding proteins with small molecules. Nat Rev Chem 4(9): 441-458.
6. Joseph BP, Weber V, Knüpfer L, Giorgetti A, Alfonso Prieto M, et al. (2023) Low Molecular Weight Inhibitors Targeting the RNA-Binding Protein HuR. Int J Mol Sci 24(17): 13127.
7. Jaiswal AK, Thaxton ML, Scherer GM, Sorrentino JP, Garg NK, et al. (2024) Small molecule inhibition of RNA binding proteins in haematologic cancer. RNA Biol 21(1): 1-14.
8. Liu J, He L, Collins I, Ge H, Libutti D, et al. (2000) The FBP interacting repressor targets TFIIH to inhibit activated transcription. Mol Cell 5(2): 331-341.
9. Page McCaw PS, Amonlirdviman K, Sharp PA (1999) PUF60: a novel U2AF65-related splicing activity. Rna 5(12): 1548-1560.
10. Hastings ML, Allemand E, Duelli DM, Myers MP, Krainer AR (2007) Control of pre-mRNA splicing by the general splicing factors PUF60 and U2AF(65). PLoS One 2(6): e538.
11. Královicová J, Ševcíková I, Stejskalová E, Obuca M, Hiller M, et al. (2018) PUF60-activated exons uncover altered 3' splice-site selection by germline missense mutations in a single RRM. Nucleic Acids Res 46(12): 6166-6187.
12. Zhang C, Ni X, Tao C, Zhou Z, Wang F, et al. (2024) Targeting PUF60 prevents tumor progression by retarding mRNA decay of oxidative phosphorylation in ovarian cancer. Cell Oncol (Dordr) 47(1): 157-174.
13. Xu N, Ren Y, Bao Y, Shen X, Kang J, et al. (2023) PUF60 promotes cell cycle and lung cancer progression by regulating alternative splicing of CDC25C. Cell Rep 42(9): 113041.
14. Sun D, Lei W, Hou X, Li H, Ni W, et al. (2019) PUF60 accelerates the progression of breast cancer through downregulation of PTEN expression. Cancer Manag Res 11: 821-830.
15. Long Q, An X, Chen M, Wang N, Sui S, et al. (2020) PUF60/AURKA Axis Contributes to Tumor Progression and Malignant Phenotypes in Bladder Cancer. Front Oncol 10: 568015.
16. Wang F, Peng L, Sun Y, Zhang B, Lu S (2022) PUF60 promotes glioblastoma progression through regulation of EGFR stability. Biochem Biophys Res Commun 636(1): 190-196.
17. Long Q, Hua Y, He L, Zhang C, Sui S, et al. (2020) Poly(U) binding splicing factor 60 promotes renal cell carcinoma growth by transcriptionally upregulating telomerase reverse transcriptase. Int J Biol Sci 16(15): 3002-3017.
18. Shoichet BK (2004) Virtual screening of chemical libraries. Nature 432(7019): 862-865.
19. Zhu H, Zhang Y, Li W, Huang N (2022) A Comprehensive Survey of Prospective Structure-Based Virtual Screening for Early Drug Discovery in the Past Fifteen Years. Int J Mol Sci 23(24): 15961.
20. Zhang C, Xu Y, Zhu X, Zhang X, Wang F, et al. (2024) Phosphorylation of FOXK2 at Thr13 and Ser30 by PDK2 sustains glycolysis through a positive feedback manner in ovarian cancer. Oncogene 43: 1985-1999.
21. Chen CY, Ezzeddine N, Shyu AB (2008) Messenger RNA half-life measurements in mammalian cells. Methods Enzymol 448: 335-357.
22. Wu T, Fu XD (2015) Genomic functions of U2AF in constitutive and regulated splicing. RNA Biol 12(5): 479-485.
23. Corsini L, Hothorn M, Stier G, Rybin V, Scheffzek K, et al. (2009) Dimerization and protein binding specificity of the U2AF homology motif of the splicing factor Puf60. J Biol Chem 284(1): 630-639.